Photochemical & Photobiological Sciences

RSC Publishing

PAPER

View Article Online
View Journal | View Issue

Cite this: *Photochem. Photobiol. Sci.*, 2013, **12**, 1855

A structural model for the full-length blue light-sensing protein YtvA from *Bacillus subtilis*, based on EPR spectroscopy†

Christopher Engelhard,[a] Sarah Raffelberg,[b] Yifen Tang,[b] Ralph P. Diensthuber,[c] Andreas Möglich,[c] Aba Losi,[d] Wolfgang Gärtner[b] and Robert Bittl*[a]

Received 26th April 2013,
Accepted 9th July 2013

DOI: 10.1039/c3pp50128k

www.rsc.org/pps

A model for the full-length structure of the blue light-sensing protein YtvA from *Bacillus subtilis* has been determined by EPR spectroscopy, performed on spin labels selectively inserted at amino acid positions 54, 80, 117 and 179. Our data indicate that YtvA forms a dimer in solution and enable us, based on the known structures of the individual domains and modelling, to propose a three-dimensional model for the full length protein. Most importantly, this includes the YtvA N-terminus that has so far not been identified in any structural model. We show that our data are in agreement with the crystal structure of an engineered LOV-domain protein, YF1, that shows the N-terminus of the protein to be helical and to fold back in between the β-sheets of the two LOV domains, and argue for an identical arrangement in YtvA. While we could not detect any structural changes upon blue-light activation of the protein, this structural model now forms an ideal basis for identifying residues as targets for further spin labelling studies to detect potential conformational changes upon irradiation of the protein.

Introduction

In recent years, biological photoreceptors have gained remarkable scientific interest, as in many of these proteins the signalling part is an enzyme activity,[1] which, in connection with the light sensing domain, suggests regulation of the specific enzyme activity by light irradiation.[2] Among the broad variety of photoreceptors, the blue light-sensing proteins are of particular interest, as (i) their flavin chromophore is endogenous in all living organisms, and (ii) one subclass of these receptors, the LOV domain-proteins (LOV, Light, Oxygen and Voltage), shows a robust three-dimensional structure and yet a broad variety of naturally occurring signalling domains.[3] The first prokaryotic LOV domain protein discovered was YtvA from *Bacillus subtilis*, a photoreceptor involved in the stress response of this bacterium.[4–6] YtvA is a relatively small protein of only 261 amino acids and is composed of two domains, the light-sensing LOV domain and a putative signalling STAS domain (STAS, Sulfate Transporter and Anti-Sigma antagonist), both domains being connected by a short helical linker. Despite intensive research into the structure and the function of YtvA,[7–11] structural information on the full-length protein is still limited.[6,8,12]

Detailed structural knowledge is clearly required, as information on a monomeric or dimeric state or on the domain arrangement of these receptors is essential for an understanding of their biological function. Relatively few spectroscopic techniques can be applied to proteins in solution for structural elucidation. Among these, Electron Paramagnetic Resonance (EPR) spectroscopy offers a number of advantages, as it is applicable for determining inter-protein distances over a wide range, and in addition, it provides information on the dynamics and flexibility of proteins[13,14] as well. For applying EPR methods, spin labels often have to be introduced into the proteins under investigation which is best accomplished *via* covalent attachment of nitrogen-oxide substituents, carrying one unpaired electron.[15–17] These label compounds selectively react with the side chain of cysteines and can be inserted selectively at single positions to probe, *e.g.*, the oligomeric state of a protein, or can be applied as couples, thus providing information on distances within one domain or one protein entity. For these approaches, cysteines are first removed from "unwanted" positions (by mutation into serines or alanines) and are inserted at the desired positions, always keeping in

[a]*Freie Universität Berlin, Fachbereich Physik, Arnimallee 14, 14195 Berlin, Germany. E-mail: robert.bittl@fu-berlin.de; Fax: +49 (30) 838-56046; Tel: +49 (30) 838-56049*
[b]*Max-Planck-Institute for Chemical Energy Conversion, Stiftstr. 34-36, 45470 Mülheim, Germany*
[c]*Humboldt Universität zu Berlin, Institut für Biologie, Biophysikalische Chemie, Invalidenstr. 42, 10115 Berlin, Germany*
[d]*University of Parma, Department of Physics and Earth Sciences, Viale G.P. Usberti n. 7/A (Parco delle Scienze), 43124 Parma, Italy*
†Electronic supplementary information (ESI) available. See DOI: 10.1039/c3pp50128k

mind to verify the functional integrity of the mutated proteins. We report here on the insertion of spin label compounds into several sites of the LOV and STAS domains of YtvA, providing information on the oligomeric state of this protein and also proposing a structural model for the full-length protein, as derived from intra- and intermolecular distances.

Results

Labelling strategy and efficiency

Labelling positions were chosen not only to determine the oligomeric state of YtvA but also to enable us to determine, based on the known crystal or homology structures for the LOV and STAS domains, the conformation of the domains within one monomer as well as the binding geometry of a potential dimer. To this end, in addition to two singly labelled mutants, several variants that were simultaneously labelled in both domains were produced. Five mutants were generated for this study, two singly labelled mutants (T117C and T179C – in all cases, the nomenclature such as T179C indicates a side chain substituted by a spin-labelled cysteine) and two doubly labelled mutants (T80C/T179C and T54C/T179C) as well as one mutant with inhibited cysteinyl-C4a-adduct formation (C62A). The positions of these sites are shown in Fig. 1. The spin label yield attached to the mutagenesis-inserted cysteine residues was determined for all five constructs and was found to be greater than 95%. Also, the extent of flavin chromophore incorporation was determined and found in all cases to be greater than 90%. A control for the photochemical properties of all mutations revealed no change caused by the mutations and the spin-labelling, including, crucially, the formation of the cysteinyl-C4a-adduct.

cw-EPR

cw-EPR experiments on various labelled mutants were carried out at ambient temperature $T \approx 295$ K in order to detect the mobility of the protein-bound labels and thereby investigate the immediate surroundings of the spin labels (Fig. 2).[17,18] Even though great care was taken to keep the sample treatment constant, a variable small amount of remaining free spin label

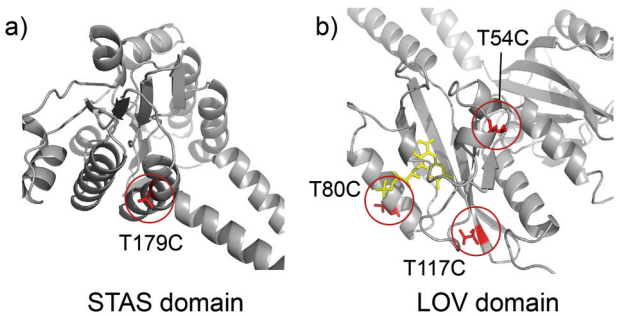

Fig. 1 Structure of the YtvA STAS (a) and LOV (b) domains with the position of the spin-labelled sites highlighted in red. The flavin cofactor, converted into the radical form in the C62A mutant, is shown in yellow.

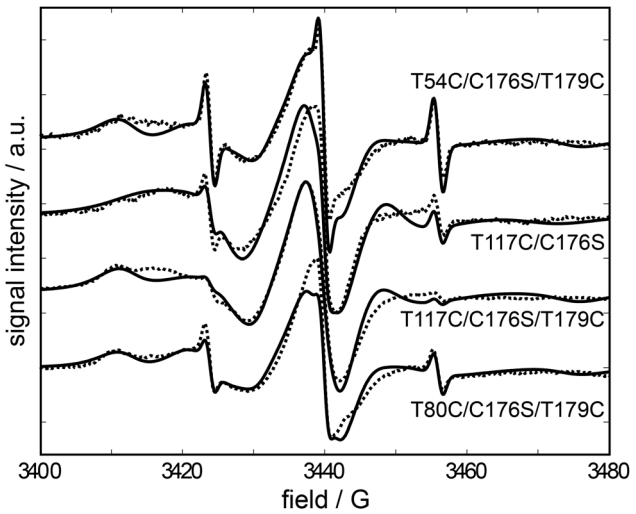

Fig. 2 X-band *cw*-spectra recorded at room temperature of the investigated mutants (solid lines) with simulations (dotted lines). The differences in label mobility are clearly visible from the moving pattern of peaks between 3405 G and 3430 G.

after washing is inevitable. Since the free spin label signal is very narrow, even a small contribution of free label gives rise to a large *cw*-EPR signal compared to the broad signal of protein-attached label. This leads to the prominent signal triplet at 3424 G, 3440 G, and 3456 G with varying intensity between samples.

The protein-bound spin labels show complex spectra with marked differences between the individual samples in the low-field part of the spectrum between 3400 G to 3430 G, indicative of strong differences in mobility between the different labels. While the spectra of all samples show a broad background in this region, implying a distribution of label mobility, signals corresponding to dominant components could be identified by comparing the spectra of the different variants. The three mutants YtvA T80C/C176S/T179C, YtvA T54C/C176S/T179C, and YtvA T117C/C176S/T179C all yield a low field peak at 3411 G, indicative of a slowly tumbling spin label. Such behaviour is not seen for YtvA T117C/C176S. This mutant, instead, shows a clear signal at 3417 G (also present, slightly shifted to lower fields, in YtvA T117C/C176S/T179C). YtvA T80C/C176S/T179C and YtvA T54C/C176S/T179C exhibit one additional peak at 3421 G and 3425 G, respectively. Especially in the case of YtvA T54C/C176S/T179C, this signal partially merges with the signal arising from the free spin label, indicating a high degree of mobility for these labels.

The observed peak patterns allow assignment of the peak at 3411 G to the label at T179C, the signal at 3417 G to T117C and the peaks at 3421 G and 3425 G to T80C and T54C, respectively. The varying peak patterns are indicative of different mobilities of the respective labels. Using simulations performed in Easyspin[19] approximate rotational correlation times indicative of the mobilities were determined. As expected, the mobilities of the labels vary strongly, with the labels at T54C, T80C, and T117C being fairly mobile while the

label at T179C is apparently almost completely immobilised by the protein backbone.

Phase memory time measurements

To further evaluate the influence of the protein backbone on the spin labels at different positions, spin relaxation experiments at low temperatures were performed to determine the phase memory time.[20] For these experiments the samples were reconstituted in a fully deuterated buffer–glycerol mixture (50% v/v) in order to minimise the effects on the spin relaxation arising purely from the solvent. The spectra shown in Fig. 3 were recorded at 70 K.

All spectra show strong nuclear modulations of the intensity over time, due to coupling of the electron spin to nearby deuterium nuclei, rendering the fitting of an exponential decay to the data difficult. However, this modulation is proportional to $1 - \sin^2(t)$, *i.e.*, it always represents a signal loss, meaning that the fit of echo decay can be extended to the region of strong modulations by selecting only the points of maximum intensity for the fit procedure. Accordingly, an automatic peak detection algorithm was employed that yielded the relaxation times (Table 1). Both doubly labelled mutants, T80C/C176S/T179C and T54C/C176ST179C, could be fitted using a double exponential; however, only for T80C/C176S/T179C two distinct components could be identified. For YtvA T117C/C176S and YtvA C176S/T179C a single exponential provided a good fit of the simulation to the data, implying that at least from the perspective of the immediate label surroundings, only one conformation of YtvA is present.

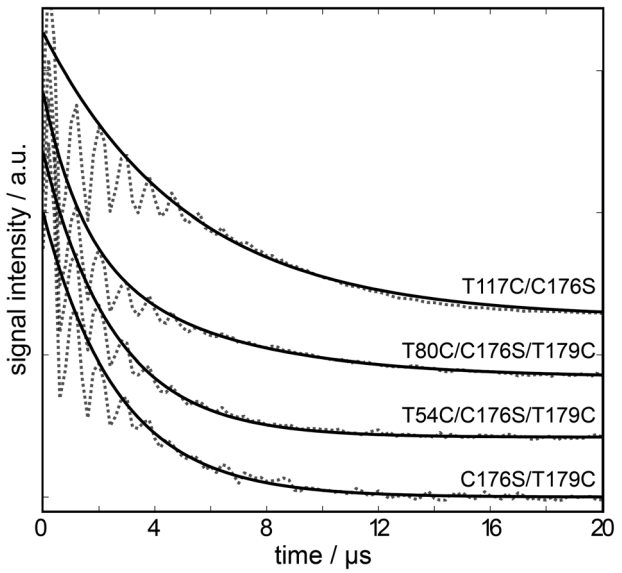

Fig. 3 Relaxation measurements performed at 70 K (solid) with fitted exponential decays (dotted). Both YtvA T54C/C176S/T179C and YtvA C176S/T179C reveal a much faster relaxation compared to YtvA T117C/C176S. The trace for YtvA T80C/C176S/T179C required a bi-exponential fit and consists of one fast component associated with the label at T179C and one slow component with relaxation times similar to the label at T117C. The resulting relaxation times are given in Table 1.

Table 1 Relaxation times of the investigated labels, measured at 70K

Sample	Relaxation time T_M/µs
T54C–T179C	1.27
T80C/T179C	0.69/2.53
T117C	2.59
T179C	1.34

While relaxation times in protonated buffer are more or less uniform for all samples (data not shown), the T_M relaxation time in deuterated buffer varies strongly from sample to sample. Both YtvA T54C/C176S/T179C and YtvA C176S/T179C show a very fast relaxation of *ca.* T_M = 1.34 µs, while the relaxation of YtvA T117C/C176S is very slow (T_M = 2.59 µs). Thus the spin labels attached to T54C and T179C are fast relaxing, pointing to a strong interaction with either protons in the protein backbone or the electron spin of another spin label close by. The label at T117C relaxes slowly, indicating that it is strongly exposed to the solvent and neither in close proximity to the protein backbone nor to other labels.

The *cw*-EPR data revealed that the spin label at T179C is strongly immobilised by (and thus in close proximity to) the protein backbone. This conclusion is corroborated by the short phase memory time. Since the spin label at T54C shows a similarly short phase memory time as T179C in spite of its high degree of mobility, it can neither be strongly exposed to the solvent nor immobilised by the backbone. We therefore conclude that the spin label is either located in close proximity to a second label or attached to the protein in a location that, while still allowing for a high degree of mobility, restricts the conformational space mainly to orientations on or close to the surface of the protein. Results from the simulation of the spin label bound to crystal structures support the latter conclusion (see the discussion below).

In the case of YtvA T80C/C176S/T179C, a biexponential decay is clearly visible in the time trace, indicative of significantly different T_M relaxation times for the two different labels. The biexponential fit of the data yields time constants of T_M = 2.53 µs and T_M = 0.69 µs for the slow and the fast component, respectively. The fast component has a shorter T_M than the value of T_M = 1.34 µs expected for the label at T179C in this mutant; however, this discrepancy is probably due to the fact that the strong nuclear modulation leaves very few significant data points in the first part of the time trace where a fast-relaxing component is most apparent. The relaxation time of the slow components places the label at T80C in a similar surrounding as the one at T117C.

Distance measurements

Two pulsed EPR methods at cryogenic temperatures were used to determine the distances between the introduced labels: (i) field swept echo (FSE) experiments to detect short label distances below 2 nm *via* the dipolar broadening of the spectrum and (ii) 4-pulse ELDOR[21] to directly detect dipolar couplings for longer distances that do not result in spectral broadening.

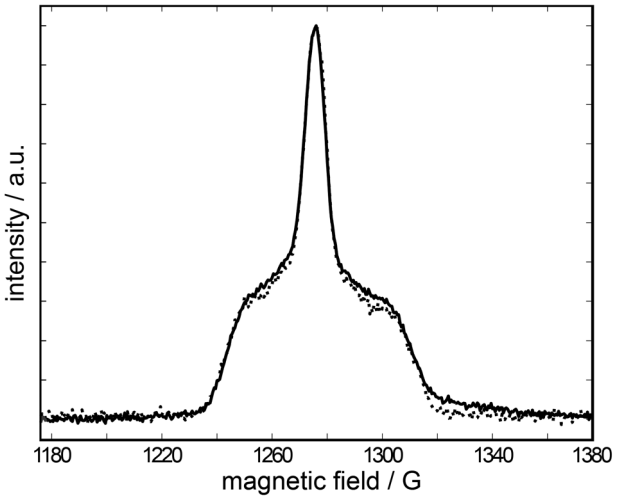

Fig. 4 S-band FSE spectrum of YtvA T54C/C176S/T179C (solid line) and YtvA T117C/C176S (dashed line) at 80 K. The spectrum of YtvA T117C/C176S is unbroadened with respect to an isolated spin label spectrum (not shown). YtvA T54C/C176S/T179C shows slight differences when compared to T117C/C176S, but no clear dipolar broadening.

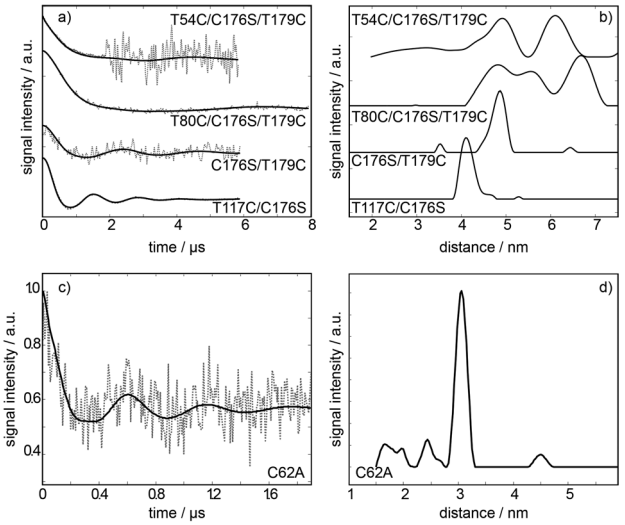

Fig. 5 (a) Background-corrected DEER spectra of spin-labelled samples recorded at 70 K (dotted lines) and DeerAnalysis fits (solid lines) and (b) inter-spin distance distributions calculated from fit in (a). (c) Background corrected DEER spectrum of the flavin radical in C62A recorded at 160 K (dotted) and fitted time trace (solid), and (d) inter-spin distance distribution calculated from the fit in (c). For YtvA T54C/C176S/T179C a composite time trace derived from measurements with 2 µs and 6 µs is shown. Both the labels at T117C and T179C reveal a clearly defined modulation (a, lower two datasets) corresponding to a very narrow distance distribution (b, lower two distributions).

Dipolar broadening in field swept echo spectra

FSE experiments were performed at the S-band to minimise the effects of g anisotropy. Of the investigated samples, only YtvA T54C/C176S/T179C showed a very small deviation from an isolated spin label spectrum (Fig. 4). The effect is too small to indicate significant dipolar broadening. Our data therefore strongly suggest that there are no distances <2 nm present in the investigated samples.

ELDOR measurements

To detect larger distances in the 2–8 nm range, 4-pulse ELDOR experiments at 70 K were performed (Fig. 5). For a singly labelled sample an exponential signal decay would be expected; however, in both samples, YtvA T117C/C176S and YtvA C176S/T179C, a distinct modulation with a period of t_{117} = 1.32 µs and t_{179} = 2.21 µs, respectively, was observed, proving conclusively that YtvA is not monomeric (Fig. 5a) under the measurement conditions. Modelling the data in DeerAnalysis, the time traces of both YtvA T117C/C176S and YtvA C176S/T179C result in a distinct, narrow distance distribution centred at d_{117} = 4.13 nm and d_{179} = 4.87 nm, respectively (Fig. 5b). The observation of a single narrow distance distribution in each of these two samples proves that YtvA is present as a dimer. The narrow distance distribution further indicates that the dimerisation is not the result of unordered or weakly ordered aggregation, but rather demonstrates the existence of a highly ordered dimerisation.

The spectra of the double mutants YtvA T80C/C176S/T179C and YtvA T54C/C176S/T179C show less pronounced modulations indicating that the distance distributions of these labels are broader compared to those of YtvA T117C/C176S and YtvA C176S/T179C. This, however, could partly be due to the dimeric nature of YtvA: since there are now four labels present in the YtvA dimer, this yields six possible label pairs, each with a corresponding distance distribution.

The distance distribution of YtvA T80C/C176S/T179C shows three different broad distance peaks, centred at d = 4.8 nm, 5.6 nm and 6.7 nm. The shortest distance is identical with the one identified as the T179C–T179C distance; however, since this peak is much broader than the one detected in YtvA C176S/T179C, it is likely that there are other contributions in this distance range as well.

The fast T_M relaxation of YtvA T54C/C176S/T179C greatly reduces the signal-to-noise ratio that could be achieved in long time traces for this sample. To be able to reliably detect small distances, a combined spectrum consisting of two 4-pulse DEER measurements, one with a 2 µs time trace and one with a 6 µs time trace, was used (Fig. 5). In this combined dataset, the signal-to-noise ratio of the first part of the time trace allowed a clear identification of a short distance at about 3 nm. Despite the use of combined spectra, large regularisation parameters were still necessary to ensure that no artefacts were introduced by the noisy second half of the time trace. Due to the limited length of the time trace, the shape of the largest-distance peak at approximately 6 nm could not reliably be interpreted.

The possibility of ELDOR distance measurements between flavin radicals has been demonstrated previously.[22] Here we successfully used this method on the flavin radical in the radical-forming mutant C62A.[23] While the long T_1 and comparatively short T_M of this radical species limited the length of the recordable time trace, a clear modulation corresponding to

a narrow distance distribution centred around 3.1 nm could be detected (Fig. 5c and d). The narrow distance distribution again corroborates the very specific dimer structure deduced from the spin-labelled variants above.

Discussion

While a previous study, using gel filtration chromatography, found that only the isolated YtvA LOV domain forms a dimer, whereas the full-length protein mainly appears in a monomeric form,[12] other studies have indicated that YtvA is mostly dimeric in solution.[6,8,24] By determining spin label distances and measurements of phase relaxation times, we present here evidence that not only supports the latter proposal, but more importantly allows us to provide quantitative information about the dimer conformation.

To better relate our data to the structural information available, domain structures with attached spin labels were created using MMM[25] and mtsslWizard.[26] The results from both programs as well as insights into the label's mobility and surroundings obtained by *cw*- and pulsed EPR allow us to validate the simulation of the label's conformational space with respect to the structure. Results from both simulation methods were mostly compatible, with the exception of the simulations for the label at T179C. Simulations shown here are derived from MMM unless otherwise noted.

Validation of the YtvA-LOV crystal structure

A LOV–LOV model for YtvA where the domains associate *via* their β-sheets has been previously proposed.[6–8] In a new crystal structure of the hybrid protein YF1, a protein combining the *B. subtilis* YtvA LOV domain with the histidine kinase domain of *Bradyrhizobium japonicum* FixL,[27,28] the two N-terminal helices of the dimer are folded back into the space between the β-sheets, while retaining the overall LOV–LOV orientation, an arrangement that had been previously suggested for a similar YtvA protein from *Bacillus amyloliquefaciens*[29] as well as for a different LOV protein from *Pseudomonas putida*.[30] When using this crystal structure as a basis for our model, calculating the distance distribution for the labels attached to T117C results in excellent agreement with the measured data (Fig. 6).

The distance between the two flavin cofactors in the dimer was calculated using the atoms with the largest spin density, *i.e.* N5 and C4a, in the YF1 structure,[28] resulting in flavin–flavin distances between 2.9 nm and 3.1 nm, which again are in excellent agreement with our measured data (Fig. 5c and d). Interpretation of the distance measurements from YtvA T80C/C176S/T179C and YtvA T54C/C176S/T179C are only possible in light of the structural model for the full-length protein. The fast relaxation and high mobility of the spin label at T54 requires that this spin label is located either in close proximity to another spin label or bound to the protein in such a way that allows for comparatively free movement of the label, while keeping most conformations close to the protein surface to explain the rapid spin relaxation. Looking at the label

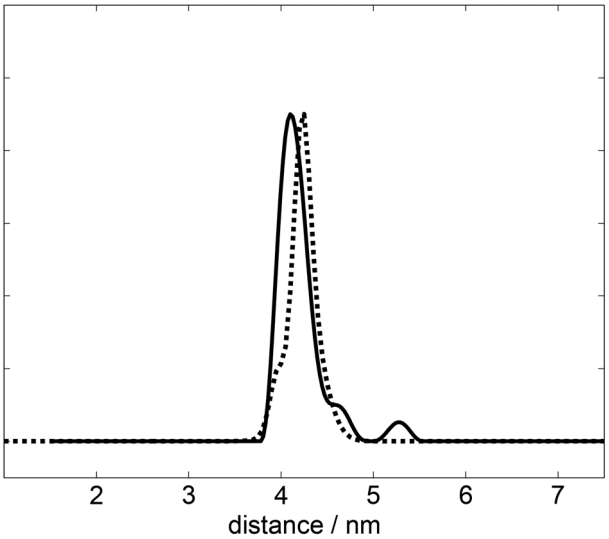

Fig. 6 MMM distance simulations for the label at T117C based on the YF1 crystal structure (dashed) compared to the experimental result (solid). The very good agreement indicates that, in solution, the LOV domains in YtvA adopt the same conformation.

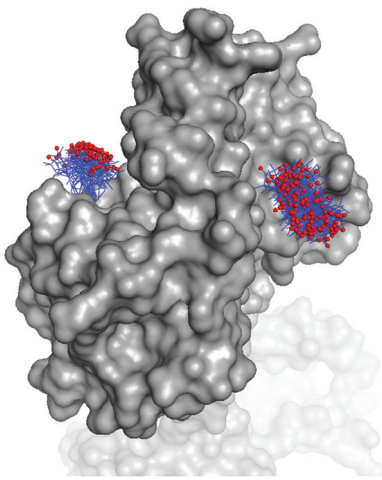

Fig. 7 Simulated spin label at T54 in the YF1 crystal structure. Shown are the various conformations the spin label can adopt. It can be seen that the label, while mobile, is flanked by the protein, bringing it into close contact with protein protons and thus reducing its relaxation times.

conformations produced by MtsslWizard (Fig. 7), it is obvious that the latter is the case: while the simulation shows a broad, continuous distribution of conformers allowing for a high degree of spin label flexibility, most of the resulting conformations show a close proximity between nitroxide and the protein surface. The alternative, two labels in close proximity, is additionally excluded by the FSE and pELDOR data, neither of which show any indication of small distances between labels.

In summary, neither the distance observed between the spin labels at T117C and between the flavin radicals, nor the observed behaviour of the spin labels attached at T54C is compatible with an LOV–LOV arrangement without the N-terminal

helices folded back between the domains, while all are in excellent agreement with the YF1 crystal structure.[28] This indicates that the LOV domains of YtvA in solution form a dimer as shown for YF1[28] as well as for the LOV domain dimer of *B. amyloliquefaciens* YtvA.[29]

Based on this LOV–LOV conformation we can now derive from our data a model for the STAS–STAS interaction and the structure of the full-length protein.

The STAS–STAS interface and a model for the full-length structure

MMM simulation of the label at T179C yielded a relatively flexible label with a large conformational space that would result in broad distance distributions (the spin label, when simulated in MtsslWizard, was both far less flexible and more narrowly distributed), while we know from *cw* experiments that this label is in fact highly *immobile*. This discrepancy is most likely due to the fact that the only available structural information for the STAS domain is a homology model. Similar calculations of the spin label conformational space in known STAS domain structures from *B. subtilis* SpoIIAA[31] and *Moorella thermoacetica*[32] confirm the susceptibility of the MMM results for this label to small changes in protein structure. Since MtsslWizard and MMM use different methods for calculating allowed conformations (sampling of the conformational space in the case of MtsslWizard and rotamer libraries in the case of MMM; for a detailed discussion see ref. 26), differences in the simulated distance distributions may be expected. In this specific case, our data from *cw* and pulsed EPR experiments showing that the label at T179C is immobilised by the protein are in better agreement with the MtsslWizard simulation, which predicts a less mobile label.

The large measured distance of 4.83 nm between the labels at T179C requires that they are facing outwards from the STAS–STAS dimer. Multiple test structures of bound STAS domains that fulfilled this condition were generated by rigid-body modelling in ZDOCK and then further ranked with respect to the T179C–T179C distance distribution and their compatibility with the structure of the linker. This rigid-body approach, both in simulating possible conformations of the STAS–STAS dimer as well as for the binding of the resulting dimer to the LOV–LOV crystal structure, allows the generation of a model for the full-length protein from relatively few distance constraints (Fig. 8).

The data obtained from ELDOR measurements of YtvA T80C/C176S/T179C and YtvA T54C/C176S/T179C were then used to align the STAS structure in relation to the LOV dimer. These calculations were performed in MMM, since MtsslWizard is less suited for the calculation of multi-spin distance distributions. However, as previously discussed, the MMM simulation overestimates the width of the T179C–T179C distance distribution. This discrepancy results in additional distance features around 4.87 nm appearing in the simulation, not present in the experimental data, which has to be taken into account when interpreting the results, shown in Fig. 9.

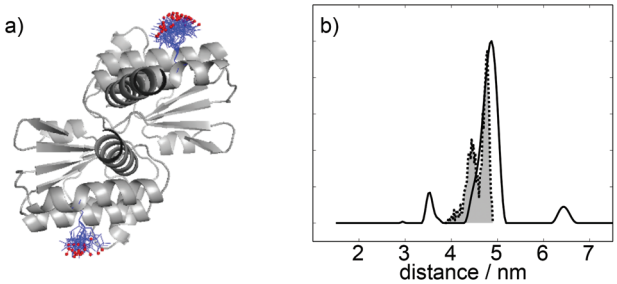

Fig. 8 (a) Model structure of the STAS–STAS dimer as derived from docking simulations with the allowed conformers of the two labels at T179C as derived from MtsslWizard. The two dark helices in the centre represent the linker peptides; the LOV domains are not shown. (b) Measured T179C–T179C distance distribution (solid) compared to the distance distribution calculated from the structure in (a) (dashed, shaded).

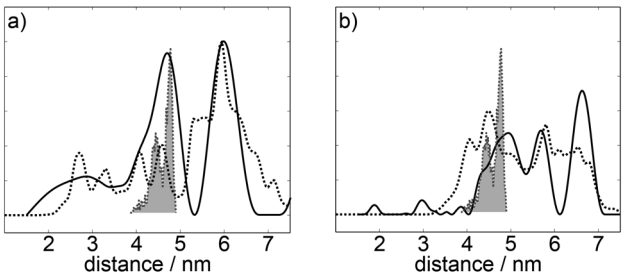

Fig. 9 Distance distributions for (a) YtvA T54C/C176S/T179C and (b) YtvA T80C/C176S/T179C. Solid: measured distribution, dotted: as calculated from the model using MMM, shaded grey: T179C–T179C distance calculated using mtsslWizard. Comparison of the calculations from MMM and mtsslWizard shows that the discrepancy around 4–5 nm in the simulated distributions can be accounted for by the too broad T179C distribution in MMM calculations.

In the case of YtvA T54C/C176S/T179C the peak at 2.7 nm corresponds to the T54C–T54C distance within the LOV dimer, the peak at 4.7 nm is the signal already previously identified as originating from the T179C–T179C interaction. Thus, the broad peak at 6 nm is the superposition of all four possible T54C–T179C pairs.

The distance distribution of YtvA T80C/C176S/T179C does not split as clearly into identifiable distances. The main discrepancy between the simulation and the measured data relates to the region around 4 nm. This, however, is again due to the overly broad distribution for T179C–T179C in the MMM simulation, as discussed above. While the experimental distance distribution does not agree with the fine structure predicted by MMM calculations, a detail which is beyond the resolution of the present experimental data, the general trimodal shapes of the distance distributions in the simulation and the measured data fit quite well. Thus, the distances observed for the T80C–T80C and T54C–T54C label pairs further strengthen the LOV–LOV binding motif derived from singly labelled variants. The STAS–STAS dimer structure derived from docking simulations in conjunction with the measured T179C–T179C distance constraint correctly reflects the distances observed for the intra-dimer label pairs T80C–T179C and T54C–T179C,

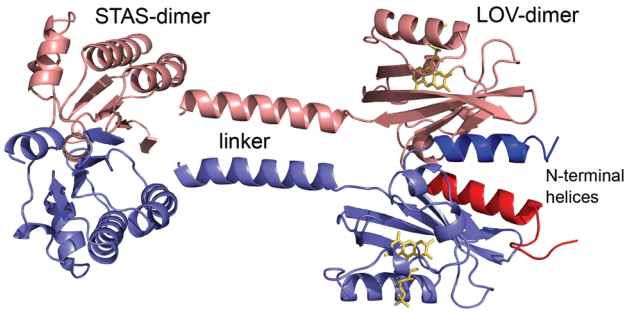

Fig. 10 Structural model of full-length YtvA, highlighting the N-terminal helices (shown in red and dark blue) between the LOV β-sheets. Five residues between the linker and the STAS-domains are not included in the structure because no data exist on their conformation.

strongly supporting the overall structure of two homo-dimers linked *via* two helices.

Conclusions

The derived structural model for the full-length protein is shown in Fig. 10. The general motif of two homo-dimers linked by two coiled helices is in very good agreement with SAXS and NMR data;[8] the major and important difference to the earlier models is the inclusion of the N-terminal helices and a different association interface for the STAS–STAS dimer.

This structural model of the full-length protein forms an ideal basis for identifying target residues for further spin labelling studies to elucidate potential conformational changes upon photo-activation.

Experimental

Sample preparation

Site-directed mutagenesis was performed as described in ref. 33. Besides the functionally active cysteine (C62), YtvA carries one other cysteine residue (position 176). This, however, was converted into a serine, as labelling studies showed that this residue is only partly accessible (≤30%). All five mutants were then based on this cys-deletion mutation (C176S). Introduced cysteines were allowed to react with (1-oxyl-2,2,5,5-tetramethyl-pyrroline-3-methyl)-methanethio-sulfonate (MTSSL) in order to attach the nitric oxide spin label. Yields of label attachment were determined *via* the Ellman test.[34] All samples were measured in a buffer containing 10 mM sodium phosphate and 10 mM NaCl at pH 8.0.

For pulsed EPR measurements, glycerol was added to a concentration of 50% (v/v) in order to slow down electron spin relaxation. To minimise the interaction between the proteins in the solvent and to further increase relaxation times, the samples were reconstituted in fully deuterated buffer/glycerol for relaxation and ELDOR experiments. Deuteration was accomplished by drying and then re-dissolving the buffer in D_2O in order to maintain the buffer at pH 8. The samples were then repeatedly exchanged with the deuterated buffer using a *Heraeus Primo R* centrifuge with *Millipore UFV5BTK00* 30 kDa membranes. In a final step deuterated glycerol was added to a final concentration of 50% v/v. The final protein concentration was between 75 μM and 100 μM.

For non-photoinduced samples, all ambient temperature experiments as well as cooling of the samples for low temperature experiments were performed in the dark to avoid photoactivation of the protein. In order to trap the adduct-inhibited mutant C62A in its radical state, the sample was first illuminated for 5 min with a high power LED at 465 nm and then rapidly frozen in liquid nitrogen.

EPR measurements

X-band EPR-measurements were performed at 9.7 GHz on Bruker BioSpin Elexsys E680 and E580 X-band spectrometers, both using a Bruker SuperX-FT microwave bridge and a Bruker ER 4118X-MD5 dielectric ring resonator. Microwave amplification for pulsed experiments was achieved with Applied Systems Engineering 117X travelling wave tube amplifiers. For ELDOR experiments the internal ELDOR microwave source of the Elexsys E580 spectrometer was used, and the E680 spectrometer was equipped with a Bruker E580-400U microwave source. S-band experiments were performed at 3 GHz on a Bruker BioSpin Elexsys E680 spectrometer with a Bruker Super-S-FTu microwave bridge and a Bruker AmpS solid state amplifier, using an ER 4118S-MS5 split-ring resonator.

cw-Spectra were recorded using 20.1 μW microwave power, 100 kHz modulation frequency and 1 G modulation amplitude. The sampling time for detection was 81.92 ms.

For field swept echo (FSE) experiments a two pulse echo sequence ($\pi/2$–τ–π–τ–echo) was employed, with pulse lengths of 40 ns and 80 ns for the $\pi/2$ and π pulses respectively. The same pulse sequence, but with a variable delay τ, was used for phase memory time measurements. For ELDOR, the four pulse DEER sequence[21] (probe pulse sequence $\pi/2$–τ_1–π–τ_1–τ_2–π–τ_2–echo with the microwave pump pulse on the second frequency being swept between the second and third probe pulses) with pulse lengths of 12 ns for the $\pi/2$ and 32 ns for the π pulses was used.

All *cw*-EPR measurements were performed at room temperature. Low temperatures for pulsed experiments were reached with *Oxford CF-935* cryostats. The temperature was controlled using *Oxford ITC503* temperature controllers for X-band and a *LakeShore 321* temperature controller for S-band measurements. Field swept echoes and relaxation experiments were performed at temperatures between 80 K and 60 K, where a temperature of 70 K was found to yield the best signal-to-noise ratio for ELDOR experiments.

Analysis

Simulation and fitting of *cw*-spectra and relaxation data was achieved in *MATLAB* using the *EasySpin* toolbox routines '*chili*' and '*exponfit*' respectively.[19] For the evaluation of ELDOR data the *MATLAB* toolbox *DeerAnalysis*[35] was used. The data were phase- and background-corrected before analysis. As a

background model a three dimensional homogeneous spin distribution was fitted to the data. Spin distance distributions were then fitted to the background-corrected spectra using Tikhonov regularisation. The resulting distance distributions were checked against modelled distances for spin label rotamers attached to the protein structure. For this, the *MATLAB* toolbox *MMM*[25] as well as the *PyMol*-plugin *MtsslWizard*[26] were used. The structure for the YtvA–LOV domain was obtained from a high resolution X-ray structure of YF1,[28] an artificial protein that incorporates both the YtvA N-terminus and LOV domain. For the STAS domain a homology model structure was used.[24] Domain docking simulations were performed in *ZDOCK*.[36]

Notes and references

1 W. R. Briggs and C.-T. Lin, Photomorphogenesis-from One Photoreceptor to 14: 40 Years of Progress, *Mol. Plant*, 2012, **5**, 531–532.
2 J. E. Toettcher, C. A. Voigt, O. D. Weiner and W. A. Lim, The promise of optogenetics in cell biology: interrogating molecular circuits in space and time, *Nat. Methods*, 2011, **8**, 35–38.
3 A. Losi and W. Gärtner, Old Chromophores, New Photoactivation Paradigms, Trendy Applications: Flavins in Blue Light-Sensing Photoreceptors, *Photochem. Photobiol.*, 2011, **87**, 491–510.
4 T. A. Gaidenko, T.-J. Kim, A. L. Weigel, M. S. Brody and C. W. Price, The blue-light receptor YtvA acts in the environmental stress signaling pathway of Bacillus subtilis, *J. Bacteriol.*, 2006, **188**, 6387–6395.
5 M. Avila-Perez, K. J. Hellingwerf and R. Kort, Blue light activates the sigma(B)-dependent stress response of Bacillus subtilis via YtvA, *J. Bacteriol.*, 2006, **188**, 6411–6414.
6 M. Avila-Perez, J. Vreede, Y. Tang, O. Bende, A. Losi, W. Gärtner and K. Hellingwerf, In Vivo Mutational Analysis of YtvA from Bacillus subtilis MECHANISM OF LIGHT ACTIVATION OF THE GENERAL STRESS RESPONSE, *J. Biol. Chem.*, 2009, 284, 24958–24964.
7 A. Möglich and K. Moffat, Structural basis for light-dependent signaling in the dimeric LOV domain of the photosensor YtvA, *J. Mol. Biol.*, 2007, **373**, 112–126.
8 M. Jurk, M. Dorn and P. Schmieder, Blue Flickers of Hope: Secondary Structure, Dynamics, and Putative Dimerization Interface of the Blue-Light Receptor YtvA from Bacillus subtilis, *Biochemistry*, 2011, **50**, 8163–8171.
9 V. Buttani, W. Gärtner and A. Losi, NTP-binding properties of the blue-light receptor YtvA and effects of the E105L mutation, *Eur Biophys. J. Biophys.*, 2007, **36**, 831–839.
10 Y. Tang, Z. Cao, E. Livoti, U. Krauss, K.-E. Jaeger, W. Gärtner and A. Losi, Interdomain signalling in the blue-light sensing and GTP-binding protein YtvA: a mutagenesis study uncovering the importance of specific protein sites, *Photochem. Photobiol. Sci.*, 2010, **9**, 47–56.
11 M. Dorn, M. Jurk and P. Schmieder, Blue News Update: BODIPY-GTP Binds to the Blue-Light Receptor YtvA While GTP Does Not, *Plos One*, 2012, **7**, E29201.
12 V. Buttani, A. Losi, T. Eggert, U. Krauss, K.-E. Jaeger, Z. Cao and W. Gärtner, Conformational analysis of the blue-light sensing protein YtvA reveals a competitive interface for LOV-LOV dimerization and interdomain interactions, *Photochem. Photobiol. Sci.*, 2007, **6**, 41–49.
13 G. W. Reginsson and O. Schiemann, Studying bimolecular complexes with pulsed electron-electron double resonance spectroscopy, *Biochem. Soc. Trans.*, 2011, **39**, 128–129.
14 Y. E. Nesmelov and D. D. Thomas, Protein structural dynamics revealed by site-directed spin labeling and multi-frequency EPR, *Biophys. Rev.*, 2010, **2**, 91–99.
15 G. L. Millhauser, Selective placement of electron-spin-resonance spin labels – new structural methods for peptides and proteins, *Trends Biochem. Sci.*, 1992, **17**, 448–452.
16 C. Altenbach, S. L. Flitsch, H. G. Khorana and W. Hubbell, Structural studies on transmembrane proteins .2. spin labeling of bacteriorhodopsin mutants at unique cysteines, *Biochemistry*, 1989, **28**, 7806–7812.
17 W. L. Hubbell, H. S. Mchaourab, C. Altenbach and M. A. Lietzow, Watching proteins move using site-directed spin labeling, *Structure*, 1996, **4**, 779–783.
18 W. L. Hubbell, C. Altenbach, C. M. Hubbell and H. G. Khorana, Rhodopsin structure, dynamics, and activation: A perspective from crystallography, site-directed spin labeling, sulfhydryl reactivity, and disulfide cross-linking, *Membr. Proteins*, 2003, **63**, 243–290.
19 S. Stoll and A. Schweiger, EasySpin, a comprehensive software package for spectral simulation and analysis in EPR, *J. Magn. Reson.*, 2006, **178**, 42–55.
20 M. Lindgren, G. R. Eaton, S. S. Eaton, B. H. Jonsson, P. Hammarstrom, M. Svensson and U. Carlsson, Electron spin echo decay as a probe of aminoxyl environment in spin-labeled mutants of human carbonic anhydrase II, *J. Chem. Soc., Perkin Trans.*, 1997, **12**, 2549–2554.
21 R. E. Martin, M. Pannier, F. Diederich, V. Gramlich, M. Hubrich and H. W. Spiess, Determination of end-to-end distances in a series of TEMPO diradicals of up to 2.8 nm length with a new four-pulse double electron electron resonance experiment, *Angew. Chem., Int. Ed.*, 1998, **37**, 2834–2837.
22 C. W. M. Kay, C. Elsässer, R. Bittl, S. R. Farrell and C. Thorpe, Determination of the distance between the two neutral flavin radicals in augmenter of liver regeneration by pulsed ELDOR, *J. Am. Chem. Soc.*, 2006, **128**, 76–77.
23 C. W. M. Kay, E. Schleicher, A. Kuppig, H. Hofner, W. Rüdiger, M. Schleicher, M. Fischer, A. Bacher and S. Weber, Blue light perception in plants - Detection and characterization of a light-induced neutral flavin radical in a C450A mutant of phototropin, *J. Biol. Chem.*, 2003, 10973–10982.
24 M. Jurk, M. Dorn, A. Kikhney, D. Svergun, W. Gärtner and P. Schmieder, The Switch that Does Not Flip: The Blue-Light Receptor YtvA from Bacillus subtilis Adopts an

Elongated Dimer Conformation Independent of the Activation State as Revealed by a Combined AUC and SAXS Study, *J. Mol. Biol.*, 2010, **403**, 78–87.

25 Y. Polyhach, E. Bordignon and G. Jeschke, Rotamer libraries of spin labelled cysteines for protein studies, *Phys. Chem. Chem. Phys.*, 2011, **13**, 2356–2366.

26 G. Hagelueken, R. Ward, J. H. Naismith and O. Schiemann, MtsslWizard: In Silico Spin-Labeling and Generation of Distance Distributions in PyMOL, *Appl. Magn. Reson.*, 2012, 42, 377–391.

27 A. Möglich, R. A. Ayers and K. Moffat, Structure and Signaling Mechanism of Per-ARNT-Sim Domains, *J. Mol. Biol.*, 2009, **385**, 1433–1444.

28 R. P. Diensthuber, M. Bommer, T. Gleichmann and A. Möglich, Full-Length Structure of a Sensor Histidine Kinase Pinpoints Coaxial Coiled Coils as Signal Transducers and Modulators, *Structure*, 2013, **21**, 1127–1136.

29 H. Ogata, Z. Cao, A. Losi and W. Gärtner, Crystallization and preliminary X-ray analysis of the LOV domain of the blue-light receptor YtvA from Bacillus amyloliquefaciens FZB42, *Acta Crystallogr. Section F-Struct. Biol. Crystal. Commun.*, 2009, **65**, 853–855.

30 F. Circolone, J. Granzin, K. Jentzsch, T. Drepper, K. E. Jäger, D. Willbold, U. Kraus and R. Batra-Saffering, Structural Basis for the Slow Dark Recovery of a Full-Length LOV Protein from Pseudomonas putida, *J. Mol. Biol.*, 2012, **417**, 362–374.

31 H. Kovacs, D. Comfort, M. Lord, I. D. Campbell and M. D. Yudkin, Solution structure of SpoIIAA, a phosphorylatable component of the system that regulates transcription factor sigma(F) of Bacillus subtilis, *Proc. Natl. Acad. Sci. U. S. A.*, 1998, **95**, 5067–5071.

32 M. B. Quin, J. M. Berrisford, J. A. Newman, A. Basle, R. J. Lewis and J. Marles-Wright, The Bacterial Stressosome: A Modular System that has Been Adapted to Control Secondary Messenger Signaling, *Structure*, 2012, **20**, 350.

33 S. Raffelberg, M. Mansurova, W. Gärtner and A. Losi, Modulation of the Photocycle of a LOV Domain Photoreceptor by the Hydrogen-Bonding Network, *J. Am. Chem. Soc.*, 2011, **133**, 5346–5356.

34 G. L. Ellman, Tissue sulfhydryl groups, *Arch. Biochem. Biophys.*, 1959, **82**, 70–77.

35 G. Jeschke, V. Chechik, P. Ionita, A. Godt, H. Zimmermann, J. Banham, C. R. Timmel, D. Hilger and H. Jung, DeerAnalysis2006 – a comprehensive software package for analyzing pulsed ELDOR data, *Appl. Magn. Reson.*, 2006, **30**, 473–498.

36 R. Chen and Z. Weng, Docking unbound proteins using shape complementarity, desolvation, and electrostatics, *Proteins*, 2002, **47**, 281–294.